

Onset of Rotational Damping in Superdeformed Nuclei

K. Yoshida and M. Matsuo*

Department of Physics, Kyoto University, Kyoto 606-01, Japan.

* *Yukawa Institute for Theoretical Physics, Kyoto University, Kyoto 606-01, Japan.*

Abstract: We discuss damping of the collective rotational motion in $A \sim 150$ superdeformed nuclei by means of a shell model combining the cranked Nilsson mean-field and the surface-delta two-body residual force. It is shown that, because of the shell structure associated with the superdeformed mean-field, onset energy of the rotational damping becomes $E_x \sim 2 - 3$ MeV above yrast line, which is much higher than in normal deformed nuclei. The mechanism of the shell structure effect is investigated through detailed analysis of level densities in superdeformed nuclei. It is predicted the onset of damping varies in different superdeformed nuclei along with variation in the single-particle structure at the Fermi surface.

1 Introduction

In recent experiments, up to around 20 different rotational bands are observed in a normally deformed rare-earth nucleus, and several superdeformed rotational bands are identified in a single superdeformed nucleus [1]. The observed rotational bands usually lie in the region near the yrast line and are often interpreted in terms of independent particle excitations in a rotating deformed mean-field. There are of course numerous excited levels at higher excitation energy, but these levels do not necessarily form rotational band structure characterized by sequences of strong E2 transitions since damping of the collective rotational motion is expected [2]. In the highly excited region, say at 1 to 2 MeV above yrast line for normally deformed nuclei, the level density at a given spin is as large as 10^2 to 10^3 MeV $^{-1}$, and the corresponding level spacing becomes comparable with or smaller than the size of matrix elements (order of 10 keV) of the residual two-body interaction. The residual interaction then becomes effective to cause mixing of many-particle many-hole configurations in the rotating deformed mean-field potential. Since different configurations respond differently to the Coriolis force due to different single-particle alignments, the configuration mixing results in loss of collectivity or damping of the collective rotational motion. Experimental data on the damping of the rotational motion are accumulating for normally deformed rare-earth nuclei from the analysis of the quasi-continuum part of gamma-ray spectra containing gamma-rays emitted from the highly excited levels [3, 4]. In particular, a fluctuation analysis of the quasi-continuum points to the presence of about 30 rotational bands in a nucleus, thus confirms occurrence of the rotational damping [3].

The mean-field models which have been very successful for rotational bands near yrast line have to be extended in order to describe the rotational damping caused by the configuration mixing effect due to the residual interaction. Such extensions can be formulated by using the shell model diagonalization on the basis of many-particle many-hole configurations associated with the cranked mean-field [5-7]. In

fact, a realistic model which combines the cranked Nilsson single-particle basis and the surface-delta residual two-body force [7] gives results consistent with the data from the fluctuation analysis method for normally deformed rare-earth nuclei. It predicts that the rotational damping sets in at around 1 MeV above yrast line.

The rotational damping in superdeformed nuclei is expected to differ significantly from that in normally deformed nuclei since the level density of superdeformed states is affected by the shell structure in the single-particle spectra [8, 9], which is the characteristic feature specific to the superdeformation. The shell-effect on the rotational damping is pointed out by an previous work [5] for ^{152}Dy , which however adopted schematic residual interaction with constant matrix elements treated as parameters. Recently, the fluctuation analysis method has been applied to a superdeformed nucleus ^{143}Eu with a first decisive and quantitative data for the onset of the rotational damping in a superdeformed nucleus [10]. It extracted an effective number of superdeformed rotational bands which is not very different from the effective number of bands in normally deformed nuclei. Since the shell structure in superdeformed nuclei is not uniform even in $A \sim 150$ region, systematic and quantitative analysis is required in order to reveal the characteristics of the rotational damping.

The present paper analyzes systematically the rotational damping in superdeformed nuclei in the $A \sim 150$ region by means of the shell model diagonalization with realistic two-body residual interaction [6]. In particular, the analysis is focused on the onset of the damping since it is most relevant to the data extracted from the fluctuation analysis method. In order to clarify the shell structure effect on the rotational damping, we also look into the level densities in detail in Section 3. It is revealed that, as consequence of the shell structure effects, the onset of damping varies in different species of superdeformed nuclei. This is because the single-particle spectra as well as the shell-gap at the Fermi surface varies as N and Z change.

2 Formulation

The microscopic model adopted in the present study is essentially the same as the formulation for normally deformed nuclei [7], except difference in the mean-field potential. In describing superdeformed states, suitable choice of the deformation parameters is important since the shell structure characteristic to superdeformation depends on the deformation.

We start with the cranked Nilsson single-particle Hamiltonian

$$\hat{h} = \hat{h}_{\text{Nilsson}} - \omega \hat{j}_x \quad (1)$$

with ω being the rotational frequency. The pairing potential is not introduced. For the Nilsson potential, the quadrupole and hexadecapole parameters ϵ_2 and ϵ_4 are considered as shape variables. We adopt the Nilsson parameters given by Ref. [11], which gives better description of proton 7_1 orbit than the parameter [12] used in Ref. [6]. The difference in the Nilsson parameters does not affect the following argument except detailed behavior. With reflection symmetry, the single-particle routhian orbits of the cranked Hamiltonian keep the parity and the signature quantum numbers. In order to guarantee smooth change in the single-particle spectrum as a function of the rotational frequency, an diabatic basis for the single-particle orbits is constructed in a similar way to Ref. [13].

An reference superdeformed configuration is defined for a given nucleus by putting

	ϵ_2	ϵ_4
^{143}Eu	0.478	0.044
^{146}Gd	0.516	0.035
^{147}Gd	0.523	0.037
^{148}Gd	0.534	0.031
^{149}Gd	0.545	0.028
^{150}Gd	0.556	0.024
^{150}Tb	0.555	0.028
^{151}Tb	0.565	0.023
^{152}Tb	0.577	0.022
^{151}Dy	0.564	0.026
^{152}Dy	0.574	0.021
^{153}Dy	0.584	0.019

Table 1: The equilibrium deformation parameters ϵ_2 and ϵ_4 at $I = 50\hbar$ determined by Strutinsky method for each superdeformed nucleus.

N neutrons and Z protons up to the Fermi surface in the diabatic single-particle spectrum. When the reference configuration is not unique due to crossings at the Fermi surface, we choose one by referring to the high- N configuration suggested from the observed yrast superdeformed band [14]. Deformation parameters (ϵ_2, ϵ_4) are determined as functions of spin by minimizing the total energy of the reference configuration with the Strutinsky shell correction defined at a given spin I [15]

$$E(I) = E^{\text{micro}}(I) - E^{\text{smooth}}(I) + E^{\text{RLD}}(I). \quad (2)$$

Here the microscopically calculated total energy is given by

$$E^{\text{micro}}(I) = \sum_{\text{occupied } i} e_i(\omega_I) + \omega_I I \quad (3)$$

with the rotational frequency ω_I given

$$J_x(\omega_I) = \sum_{\text{occupied } i} j_{xi}(\omega_I) = I, \quad (4)$$

and $e_i(\omega)$ and $j_{xi}(\omega)$ being the diabatic single-particle routhian energy and expectation value of \hat{j}_x . The Strutinsky smoothed total energy is given by

$$E^{\text{smooth}}(I) = \sum \tilde{e}_i(\tilde{\omega}) + \tilde{\omega} I \quad (5)$$

and

$$\tilde{J}_x(\tilde{\omega}) = \sum \tilde{j}_{xi}(\tilde{\omega}) = I, \quad (6)$$

with $\tilde{e}_i, \tilde{j}_{xi}$ being e_i, j_{xi} weighted by the smoothed occupation number \tilde{n}_i [16]. The rotating liquid-drop energy $E^{\text{RLD}}(I)$ is calculated according to Ref. [17]. The deformation parameters thus determined are listed in Table. 1 at a representative spin $I = 50\hbar$. The spin dependence of the deformation is weak in all the nuclei under consideration, *e.g.* $(\epsilon_2, \epsilon_4) = (0.577, 0.010) \sim (0.5700, 0.030)$ for $I = 10 \sim 70\hbar$ in ^{152}Dy . An example of the calculated cranked Nilsson spectra with the optimized deformation is shown in Fig. 1 for ^{152}Dy .

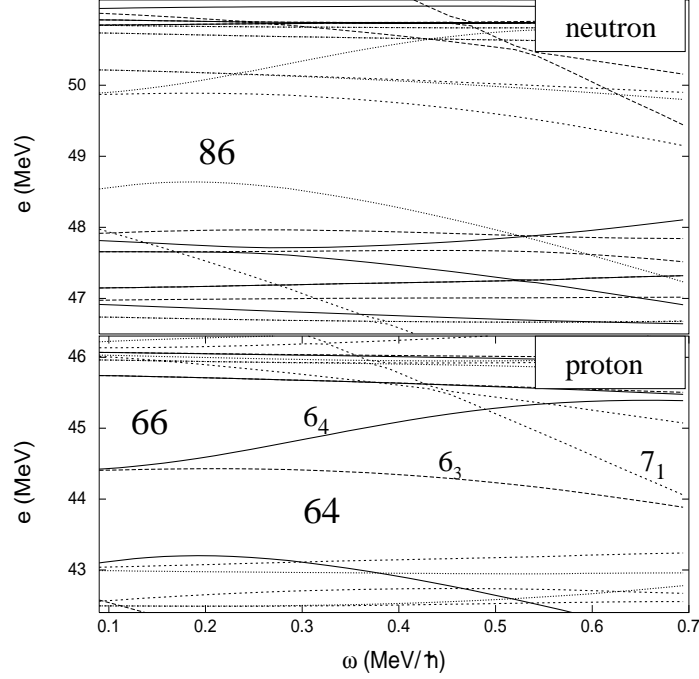


Figure 1: The single-particle routhian spectra for ^{152}Dy with the equilibrium deformation determined by the energy minimization. The deformation parameters (ϵ_2, ϵ_4) change continuously from $(0.577, 0.010)$ at $\omega = 0.07(\text{MeV}/\hbar)$, $I = 10\hbar$ to $(0.570, 0.030)$ at $\omega = 0.74(\text{MeV}/\hbar)$, $I = 70\hbar$.

In a superdeformed nucleus, there are usually more than two coexisting local minima of the total energy surface in the deformation parameter space, which correspond to superdeformed and weakly deformed mean-fields. If the mean-fields are stable (the minima are deep), excited states are expected to be built upon each mean-field. At high spins ($I \gtrsim 40\hbar$) where the superdeformed minimum becomes the lowest, states near the yrast line are dominated by excited superdeformed states.

The basis for the excited superdeformed states is formed by many-particle many-hole (np - nh) configurations in the diabatic cranked Nilsson orbits which cover the energy range $\delta E = \pm 4.8\text{MeV}$ above and below the Fermi surface. The deformation parameters and rotational frequency specifying the single-particle basis for np - nh configurations are taken common to those for the reference configuration. Energy of the basis states is given by Eq. (2), in which the microscopic energy is given for each np - nh configuration (labeled by μ) in the same way as in Ref. [8], *i.e.*,

$$E_{\mu}^{\text{micro}}(I) = E_{\mu}(\omega_I) + \omega_I I + \frac{1}{2\mathcal{J}_{\mu}^{\text{micro}}}(I - J_{x\mu}(\omega_I))^2 \quad (7)$$

where

$$E_{\mu}(\omega_I) = \sum_{\substack{\text{occupied } i \\ \text{in } \mu}} e_i(\omega_I) \quad (8)$$

and

$$\mathcal{J}_{\mu}^{\text{micro}} = \sum_{\substack{\text{occupied } i \\ \text{in } \mu}} \left. \frac{dj_{xi}(\omega)}{d\omega} \right|_{\omega=\omega_I} \quad (9)$$

is the dynamic moment of inertia of the configuration μ . The Strutinsky renormalization is important not only to determine the deformation but also to describe gamma-ray energies of the collective E2 transitions. The basis of the excited superdeformed states is denoted as $\{|\mu(I)\rangle\}$ with the energy $\{E_\mu(I)\}$. It keeps good quantum numbers with respect to the total signature and parity. Excited states built upon weakly deformed mean-fields are neglected in the present paper. At low spins ($I \lesssim 40\hbar$), they may dominate the yrast structure and the superdeformed states are to be surrounded by these weakly deformed states, while coupling between the superdeformed and weakly deformed excited states is expected to be weak if there exists a potential barrier between the local minima. We neglect the presence of the weakly deformed states since the coupling is hardly treated by a shell model description. Hereafter the yrast line refers to an envelope of the lowest energy superdeformed states as a function of spin.

For the residual two-body interaction, it is natural to assume that the effective nuclear force is not dependent on the deformation. We adopt the same surface-delta interaction (SDI) [18] with the same strength as used for describing the rotational damping in normally deformed nuclei so that results here can be compared with those for normally deformed nuclei [7]. The strength of SDI is $V_0 = 27.5/A(\text{MeV})$, which is taken from Ref. [19]. The two-body interaction is decomposed into mean-field part associated with the reference configuration and its residual, and only the residual two-body force is taken into account. The residual interaction causes configuration mixing among the basis states $\{|\mu(I)\rangle\}$ and generates energy eigenstates $|\alpha(I)\rangle$ of the many-body Hamiltonian,

$$|\alpha(I)\rangle = \sum_{\mu} X_{\mu}^{\alpha}(I) |\mu(I)\rangle \quad (10)$$

whose amplitudes are determined by numerical diagonalization. The diagonalization is done separately for each spin and parity with the lowest 700 basis states.

The E2 operator associated with the collective rotation is given by

$$\langle \mu(I) | M(E2, \lambda = 2, \mu_x = 2) | \mu'(I-2) \rangle = \sqrt{\frac{15}{128\pi}} Q_0 \delta_{\mu\mu'}, \quad (11)$$

assuming that the collective E2 transition takes place between states having the same microscopic configuration. Static quadrupole moment Q_0 is assumed to be constant for all configurations. The E2 strength for the transition from a level α at I to a level β at $I-2$ is given by

$$M_{\alpha I \beta I-2}^2 = \frac{15}{128\pi} Q_0^2 w_{\alpha \rightarrow \beta} \quad (12)$$

with normalized strength

$$w_{\alpha \rightarrow \beta} = \left(\sum_{\mu} X_{\mu}^{\alpha*} X_{\mu}^{\beta} \right)^2, \quad (13)$$

$$\sum_{\beta} w_{\alpha \rightarrow \beta} = 1. \quad (14)$$

3 Level density

In this section, we discuss characteristics of level densities of superdeformed nuclei. Since our purpose is to understand mechanism of the configuration mixing and

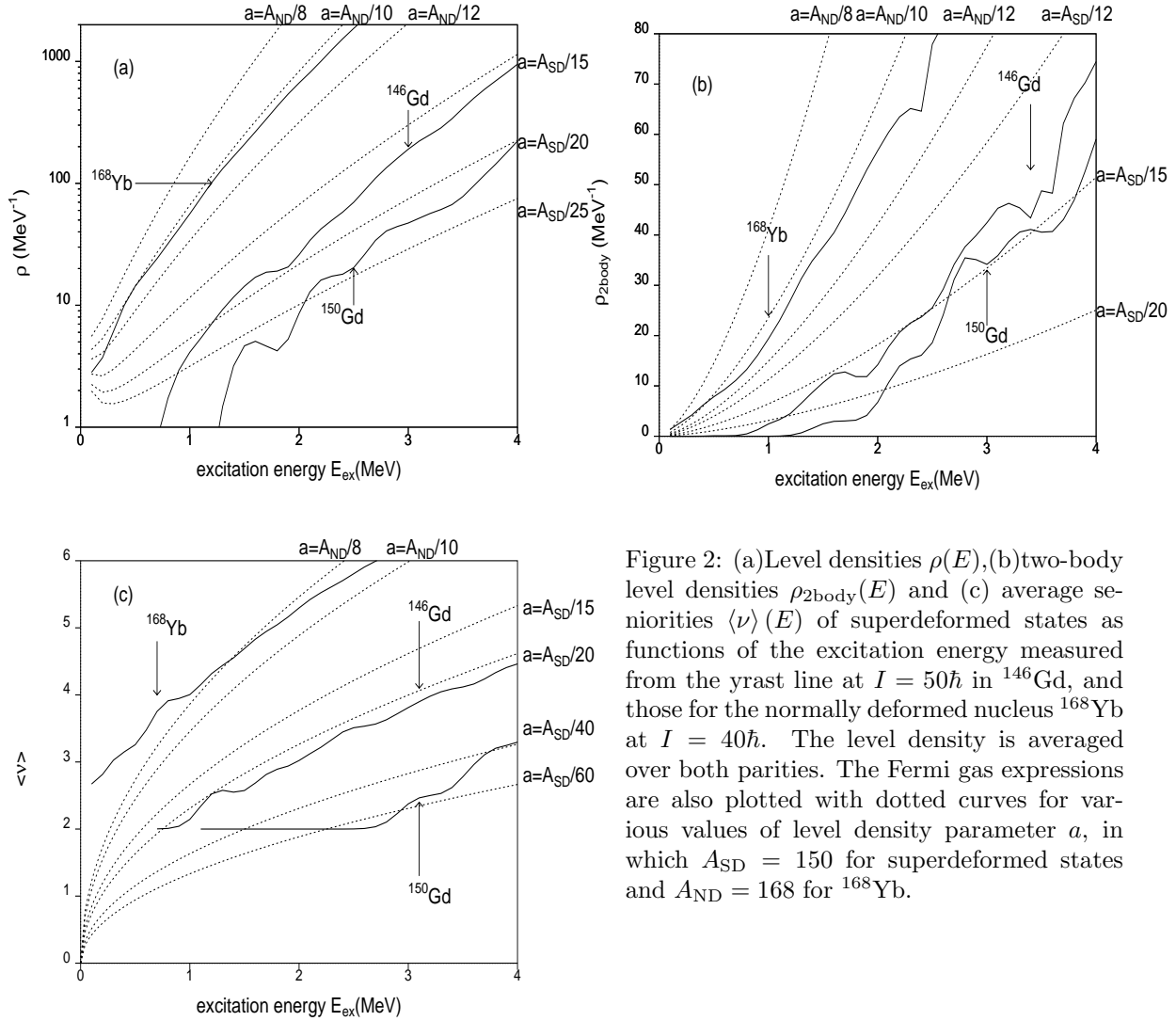


Figure 2: (a) Level densities $\rho(E)$, (b) two-body level densities $\rho_{2\text{body}}(E)$ and (c) average seniorities $\langle\nu\rangle(E)$ of superdeformed states as functions of the excitation energy measured from the yrast line at $I = 50\hbar$ in ^{146}Gd , and those for the normally deformed nucleus ^{168}Yb at $I = 40\hbar$. The level density is averaged over both parities. The Fermi gas expressions are also plotted with dotted curves for various values of level density parameter a , in which $A_{\text{SD}} = 150$ for superdeformed states and $A_{\text{ND}} = 168$ for ^{168}Yb .

the rotational damping, we deal with the level densities before the shell model diagonalization, *i.e.*, all the calculations in this section refer to the unperturbed basis states $\{|\mu(I)\rangle\}$ and their energies $\{E_{\mu}(I)\}$. Fig. 2(a) shows calculated level density of superdeformed states and compares it with the level density in a typical normally deformed nucleus ^{168}Yb . The calculated level density of super-deformed states is systematically much lower by an order of magnitude than that of normally deformed states. A similar results is obtained in the previous analysis [8, 9]. This is attributed to the low level density of the single-particle levels at the Fermi surface (See Fig.1), which is an general feature intrinsic to the superdeformed single-particle potential. In order to give quantitative discussion, the calculated level density is compared in Fig. 2(a) with the Fermi-gas expression[20, 8]

$$\rho(E) = \frac{\sqrt{\pi}}{48} a^{-\frac{1}{4}} E^{-\frac{5}{4}} \exp 2\sqrt{aE} \quad (15)$$

where the level density parameter a is supposed to be reduced and is treated as a variable parameter. The level density in the normal deformed nucleus ^{168}Yb is well fitted by the Fermi-gas expression with the level density parameter $a = \frac{\pi^2}{6} g_0 \sim A/10$,

	$A/a_{\text{tot}}[\text{MeV}]$	$A/a_{2\text{body}}[\text{MeV}]$	$A/a_{\text{seniority}}[\text{MeV}]$	$E_{\text{shell}}[\text{MeV}]$
^{143}Eu	18.5	14.9	25.2	3.56
^{146}Gd	17.6	15.0	15.9	3.94
^{147}Gd	17.5	14.2	28.0	4.02
^{148}Gd	19.1	14.6	30.8	4.31
^{149}Gd	19.4	14.1	33.8	4.59
^{150}Gd	23.9	17.0	56.2	5.14
^{150}Tb	19.0	15.1	30.3	4.43
^{151}Tb	22.6	16.4	36.6	5.08
^{152}Tb	18.2	13.4	23.0	4.53
^{151}Dy	13.8	12.3	14.8	3.09
^{152}Dy	18.9	16.6	26.7	4.55
^{153}Dy	15.9	12.1	20.3	4.19

Table 2: The level density parameters a_{tot} , $a_{2\text{body}}$, $a_{\text{seniority}}$, which are obtained by a fit to the calculated level density $\rho(E)$, the two-body level density $\rho_{2\text{body}}(E)$, and the average seniority $\langle\nu\rangle(E)$ at $E = 2.5$ MeV and $I = 50\hbar$. Since the level density parameter is often expressed as $a = A/a_0$, the table lists the value of a_0 in unit of MeV instead of a . The fifth column lists the shell correction energy $E_{\text{shell}} = -(E^{\text{micro}} - E^{\text{smooth}})$.

which agrees with the standard estimate of the single-particle level density g_0 [20]. In contrast, the calculated level density of superdeformed states corresponds to much smaller value around $a = A/15 \sim A/25$. It is known from fitting experimental data to the Fermi gas formula that the level density parameter in spherical closed shell nuclei is sizably smaller than the over-all systematics[20].

Another level density function which counts the states connected by the two-body residual interaction plays an important role in the configuration mixing of unperturbed states[2]. This quantity, which we call the two-body level density $\rho_{2\text{body}}(E)$ in the following, can be calculated explicitly as described in Appendix. The result is depicted in Fig. 2(b) and is also compared with the $\rho_{2\text{body}}$ in normally deformed ^{168}Yb and the Fermi-gas estimate for a fixed spin and parity[2]

$$\rho_{2\text{body}} = \frac{81}{4\pi^6} a^{5/2} E^{3/2}. \quad (16)$$

The two-body level density for superdeformed states is again much lower than that in the normally deformed nucleus. The corresponding value of the level density parameter is around $A/12$ to $A/20$.

Fig. 2(c) shows that average seniority (average number of particles and holes excited from the reference configuration). This quantity for superdeformed states is also significantly low in comparison with the normally deformed. The level density parameter $a_{\text{seniority}}$ which is obtained by a fit to the Fermi gas expression [21, 8]

$$\langle\nu\rangle = \log 4 \left(\frac{36}{\pi^4} a E \right) \quad (17)$$

is very low, ranging around $A/15$ to $A/60$. The level density parameters a_{tot} , $a_{2\text{body}}$ and $a_{\text{seniority}}$ obtained from the calculated $\rho(E)$, $\rho_{2\text{body}}(E)$, and $\langle\nu\rangle(E)$ are listed in Table. 2.

It should be emphasized that the level densities $\rho(E)$ and $\rho_{2\text{body}}(E)$, and the average seniority $\langle\nu\rangle(E)$ for superdeformed states are not well fitted by the Fermi-gas

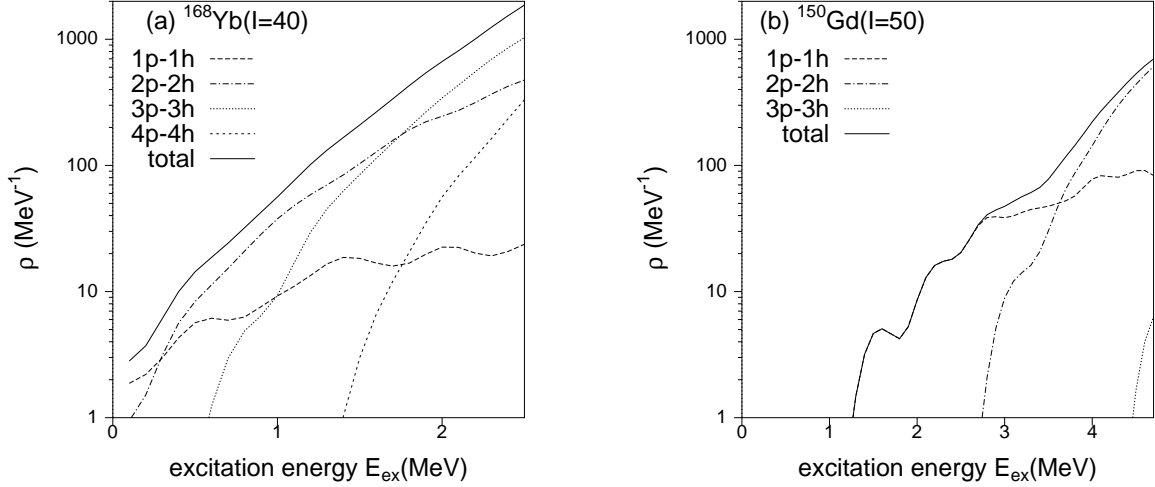


Figure 3: The level density of unperturbed np - nh configurations for (a) normally deformed nucleus ^{168}Yb at $I = 40\hbar$ and (b) superdeformed ^{150}Gd at $I = 50\hbar$ as a function of the excitation energy measured from the yrast line. In ^{150}Gd only 1p-1h and 2p-2h components are dominant for $E_{\text{ex}} < 3$ MeV, while in ^{168}Yb 1p-1h to 4p-4h contributes to the level density at the same energy region.

formulas with a single value of a for the superdeformed states. Apparently the excitation energy dependence of the calculated level densities deviates from the Fermi gas formula in the excitation energy range displayed in Fig. 2. For example, the total density $\rho(E)$ increases very slowly for $E < 1$ MeV while it shows steeper increase at $E > 1$ MeV than the fitted Fermi gas formula. It is also noticed that the level density parameter, say a_{tot} , which fits the calculated level density ρ at a given excitation energy differs from the parameter $a_{2\text{body}}$ fitting $\rho_{2\text{body}}$ and from $a_{\text{seniority}}$; a_{tot} is systematically smaller than $a_{2\text{body}}$, and $a_{\text{seniority}}$ being further smaller than a_{tot} . These features clearly indicate that the level densities of the superdeformed states cannot be represented by the Fermi gas model. The deviation between a_{tot} and $a_{\text{seniority}}$ is previously pointed out[8].

In order to understand the deviation from the Fermi gas model, it is useful to classify the excited states in terms of the number of excited particles and holes. The decomposed level densities are shown in Fig. 3 for superdeformed states ^{150}Gd as well as for normally deformed ^{168}Yb . In ^{168}Yb , there are contributions from 1p-1h to 4p-4h states for excitation below 3 MeV, while only 1p-1h and 2p-2h states contribute in the same energy region in superdeformed ^{150}Gd . Superdeformed states with 3p-3h and higher np - nh configurations lie at higher energy region. Note that the shell structure in superdeformed nuclei produces the gap of about 1 MeV at the Fermi surface in the single-particle spectrum, because of which each particle-hole excitation costs at least about 1 MeV of excitation energy. Such a feature cannot be represented by the Fermi gas model which assumes uniform single-particle spectrum.

The difference between a_{tot} and $a_{2\text{body}}$ is also explained by the presence of shell gap. The level density of np - nh states depends on excitation energy as $\rho_{npnh} \propto E^{2n-1}$ for an equidistant single particle spectrum[21], which is modified as $\rho_{npnh} \propto (E - n\Delta)^{2n-1}$ by the presence of the gap Δ at the Fermi surface. The decrease of the density due to the gap becomes very significant for np - nh states with large n . On the other hand, we find from similar decomposition of the two-body level density that the major

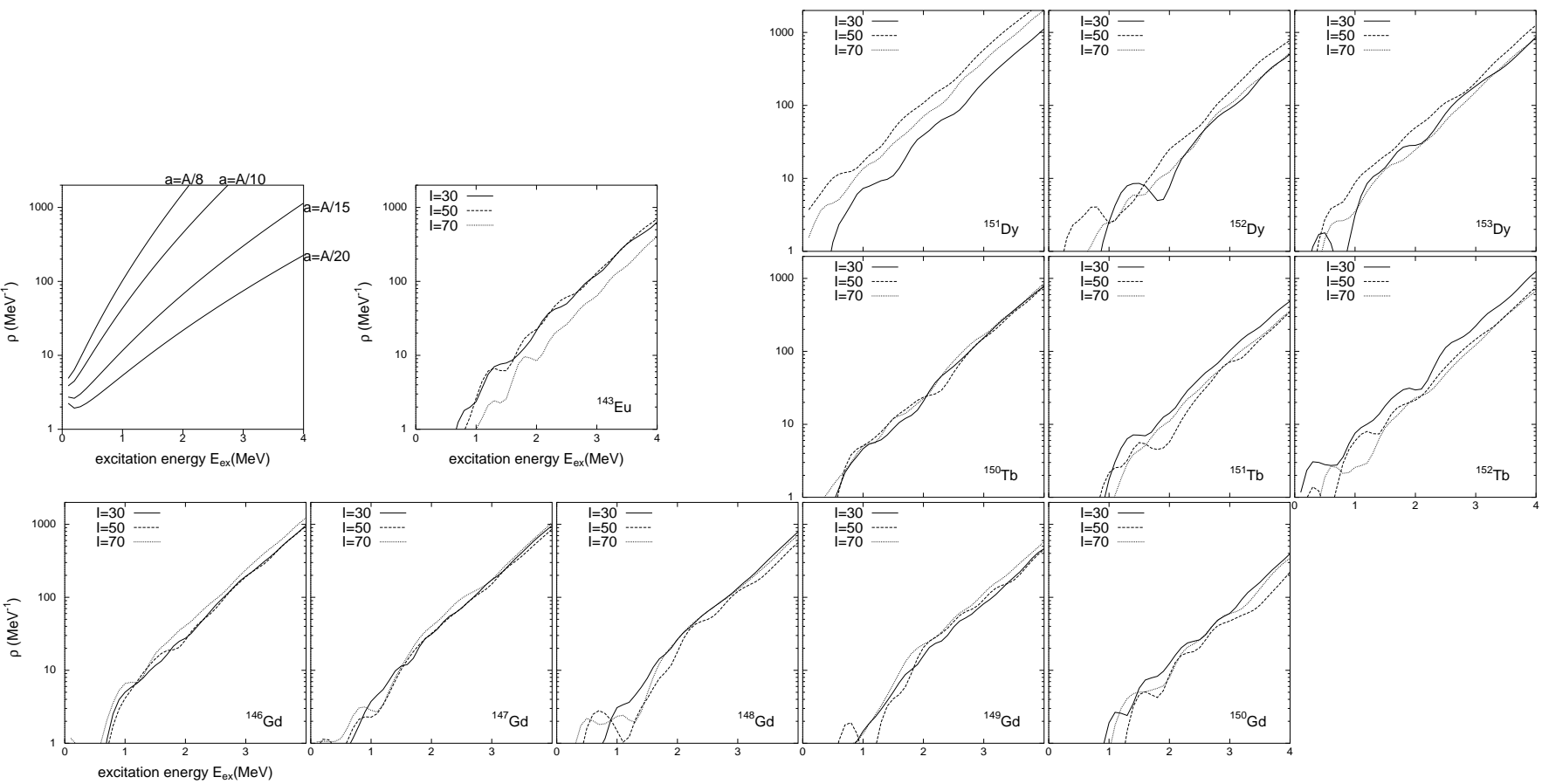


Figure 4: The level density of superdeformed states in $A \sim 150$ nuclei as a function of the excitation energy measured from the yrast line, averaged over both parities and signature states at spin I and $I+1$ for $I = 30, 50, 70\hbar$ ($I = \frac{59}{2}, \frac{99}{2}, \frac{139}{2}$ for odd nuclei). The Fermi gas formula are displayed in the left-top panel with several a parameters where $A = 150$.

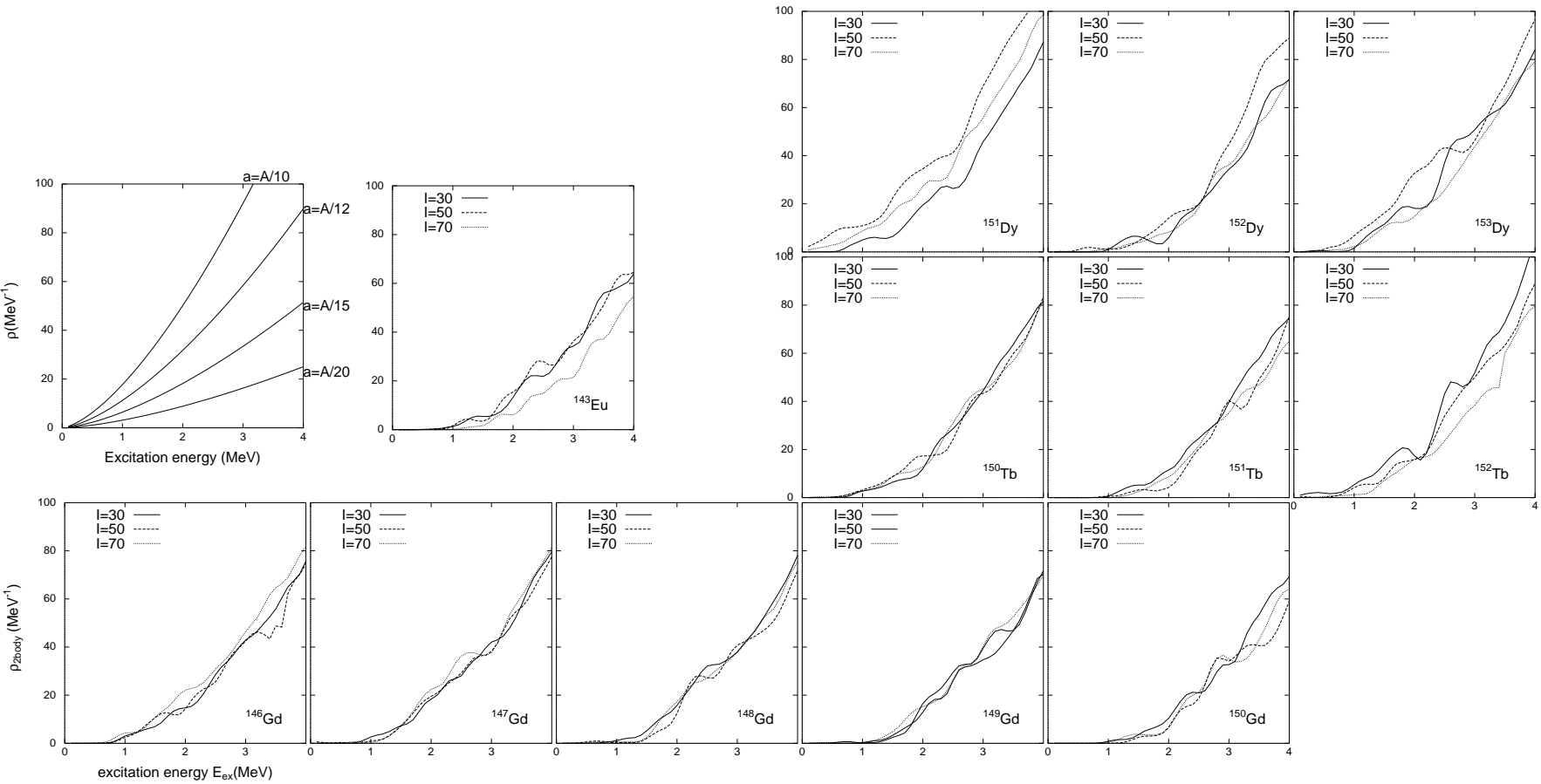


Figure 5: The two-body level density for superdeformed states in $A \sim 150$ nuclei as a function of the excitation energy measured from the yrast line, averaged over both parities and signature states at spin I and $I+1$ for $I = 30, 50, 70\hbar$ ($I = \frac{59}{2}, \frac{99}{2}, \frac{139}{2}$ for odd nuclei). The Fermi gas formula are displayed in the left-top panel with several a parameters where $A = 150$.

contribution to $\rho_{2\text{body}}$ comes from the component representing the interaction of 1p-1h to 1p-1h and 2p-2h to 2p-2h states. The subcomponent associated with the interaction among $n\text{p}n\text{h}$ states depends only linearly on energy as $\rho_{2\text{body},n\text{p}n\text{h}} \propto (E - n\Delta)^1$. Thus the gap is less effective for $\rho_{2\text{body}}$ than for ρ_{tot} , explaining the result shown in Fig. 2 and Table. 2 that the level density parameter a_{tot} fitting the total level density ρ is systematically smaller than $a_{2\text{body}}$ of the two-body density $\rho_{2\text{body}}$.

The calculated level densities of superdeformed states in $A \sim 150$ region are plotted in Fig. 4 and 5. Sizable change in the level densities depending on neutron and proton number N and Z is remarkable. For example, there is variation of more than factor 2 in the total density $\rho(E)$. The fitted level density parameters a_{tot} and $a_{2\text{body}}$ vary 50% as shown in Table. 2. The variation of the level densities should be originated from the changes in the single-particle structure in different superdeformed nuclei, which are associated with the changes in the Fermi surface and the deformation. In order to demonstrate the correlation between the level densities and the single-particle structure, we compare in Table. 2, systematics of the fitted level density parameters with that of the shell correction energy $E_{\text{shell}} = -(E^{\text{micro}} - E^{\text{smooth}})$ of the reference configuration, which is a measure of the shell effects in the single-particle spectrum. The correlation is clear in Table. 2; the larger is the shell correction energy, the smaller become the fitted level density parameters a_{tot} and $a_{2\text{body}}$. Taking Gd isotopes as an example, the level densities increase as the neutron number decreases from 86 to 82. Correspondingly the shell correction energy decreases for lighter isotopes. This can be related to both the neutron and the proton single-particle routhian structure. In ^{150}Gd , the routhian spectra are not very different from Fig. 1. The neutron and the proton spectra has a large gap at $N = 86$ and $Z = 64$ Fermi surface, respectively. For lighter Gd isotopes, the Fermi surface is situated at one to several orbits below the $N = 86$ gap, where the single-neutron level density is rather high. Furthermore the proton gap at $Z = 64$ Fermi surface decreases as the quadrupole deformation decrease (from $\epsilon_2 = 0.556$ at ^{150}Gd to $\epsilon_2 = 0.510$ at ^{146}Gd). Both effects cause the increase of level density and the decrease of the shell correction energy for lighter Gd isotopes. Another example is ^{151}Dy , in which the level density is the largest among the calculated nuclei. This is because there is no big gap in the neutron spectrum at $N = 85$ Fermi surface, and the proton gap at $Z=66$ is not very large (The proton gap for ^{151}Dy is smaller than that in Fig. 1 because of smaller quadrupole deformation). In a few nuclei, the calculated level densities show dependence on spin of about factor 2. The significant spin dependence is also attributed to the changes in the shell gap. For example, in ^{151}Dy , the $Z=66$ proton gap just above the 6_4 orbit decreases with increasing rotational frequency up to $\omega \approx 0.5\text{MeV}/\hbar$ because of the signature splitting of $6_3, 6_4$ orbits (This behavior is seen in Fig. 1).

4 Onset of rotational damping

4.1 Results

Every unperturbed many-particle and many-hole configuration created upon the cranked single-particle orbits would form a superdeformed rotational band if there were no configuration mixing. The unperturbed rotational bands are displayed in the upper panel of Fig. 6 for the signature and parity quantum number $(0, +)$ in ^{152}Dy . The lowest band has the configuration filling the single-particle orbits up to the Fermi level at $N=86$ and $Z=66$ (See Fig. 1), which corresponds to the observed

yrast superdeformed band. The second lowest band is a proton 1p-1h configuration with the hole at the 6_4 orbit and the particle at $[413]_{\frac{5}{2}}$. Other unperturbed bands displayed in the figure have mostly 1p-1h and 2p-2h configurations.

With the residual two-body interaction included, the unperturbed configurations are mixed to form energy eigenstates. The resultant energy levels are plotted with little horizontal bars in the lower panel of Fig. 6 for $(0,+)$ states in ^{152}Dy . The configuration mixing due to the residual interaction is strongly dependent on the excitation energy. An eigenstate near the yrast consists mostly of a single dominant configuration, while a state at high excitation energy consists of many unperturbed configurations. Correspondingly, the E2 decay from a near-yrast level at I feeds to a level at $I-2$ containing the same dominant component. The associated E2 strength exhausts most of the total strength for the collective rotation. The solid lines connecting the levels in Fig. 6 correspond to such strong E2 transitions. On the other hand, the E2 strength for higher excited levels is fragmented over small components decaying to many final states. A sequence of the strong collective E2 transitions (solid lines) indicates a rotational band structure. The band structure is dominant near the yrast line while it tends to disappear as the excitation energy increases, indicating the onset of the rotational damping.

In order to make a systematic analysis of the onset of rotational damping, let us discuss the excitation energy where the damping sets in. It is useful to define the branching number[6]

$$n_{\text{branch}}(\alpha) \equiv \left(\sum_{\beta} w_{\alpha \rightarrow \beta}^2 \right)^{-1} \quad (18)$$

associated with the E2 strength for decays from a level α . Here $w_{\alpha \rightarrow \beta}$ is the normalized E2 strength, Eq. (13), from a level α at I to a level β at $I-2$. This quantity measures effectively the number of E2 decay branches. The onset of the damping can be defined by the condition that the E2 decays have more than two branches or $n_{\text{branch}} > 2$ [6, 7]. An example of the calculated n_{branch} is plotted in Fig. 7 as a function of the excitation energy measured from the yrast line. The branching number increases with excitation energy, and the onset energy of the damping E_{onset} where n_{branch} exceeds 2 is given as 1.8 MeV in this example. The calculated onset energy is shown in Fig. 8 as a function of spin for superdeformed nuclei in $A \sim 150$ region.

Because of the onset of the rotational damping, there exist only limited number of rotational bands which show up as the regular sequences of levels connected with strong collective E2 transitions. The number of rotational bands thus gives a quantitative measure of the onset of the damping. Noticeably, there exist many ‘‘rotational bands with short length’’ in which strong E2 transitions continue only for two or three steps. In defining the number of rotational bands, we count the bands with length more than two. This definition corresponds to the experimental definition of the effective number of paths [4] which is extracted from the spectral fluctuation at the first ridge of the $E_{\gamma_1} \times E_{\gamma_2}$ spectra, which are formed by two consecutive E2 transitions along rotational bands. In practice, we require that along a rotational band the strong collective E2 transitions continue at least two steps with the criterion $n_{\text{branch}} < 2$. Counting those levels satisfying this condition for all parities and signatures, say $I^\pi = 40^+, 40^-, 41^+, 41^-$, we define the number of bands N_{band} at a representative spin, $40\hbar$ in this example.

The result is plotted in Fig. 9. The fluctuations in the calculated N_{band} depending on spin arise from the sharp boundary $n_{\text{branch}} < 2$ defining rotational bands, and

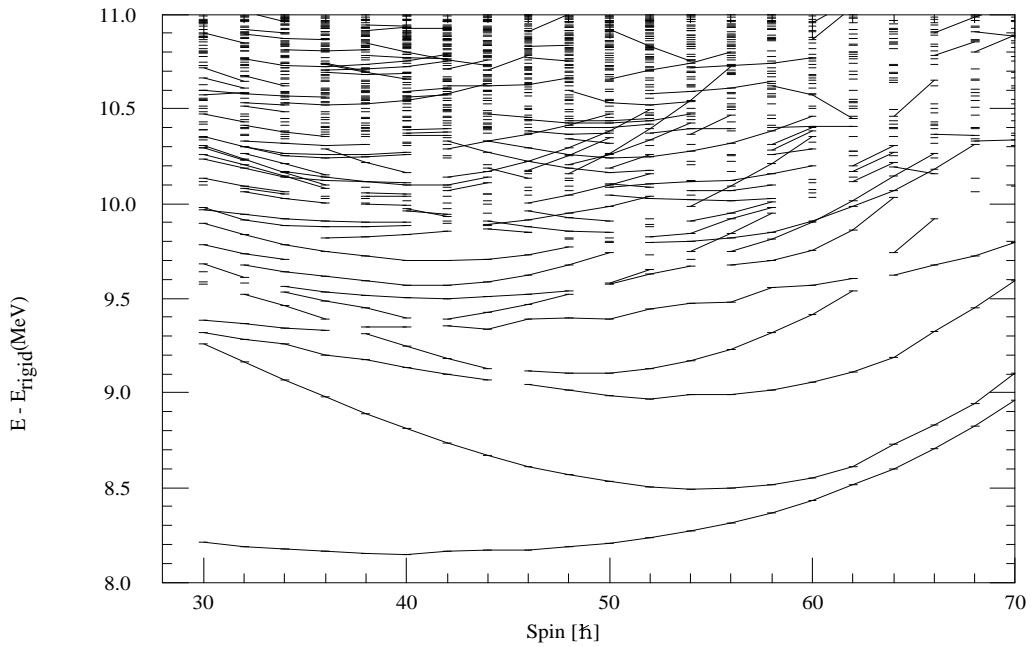
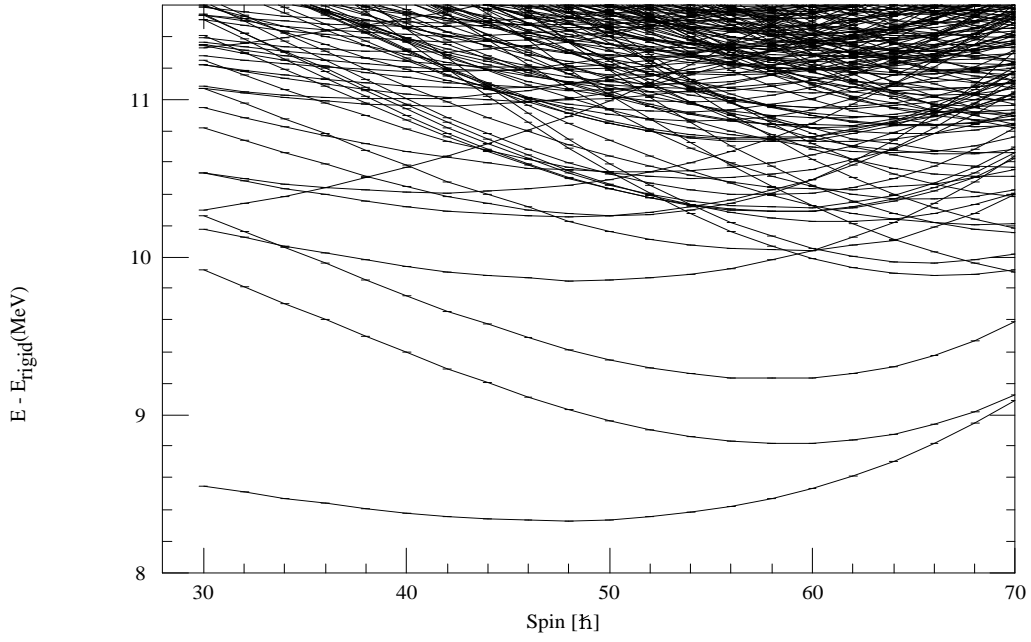


Figure 6: The calculated energy levels plotted with little horizontal bars for $(0,+)$ states in ^{152}Dy . A rigid-rotor rotational energy $E_{\text{rigid}} = I(I+1)/190$ (MeV) is subtracted. Solid lines connecting the energy levels represent strong E2 transitions with normalized strength larger than $\sqrt{1/2} = 0.707$. The upper panel shows unperturbed levels with no residual interaction. The lower panel shows the results with the residual interaction.

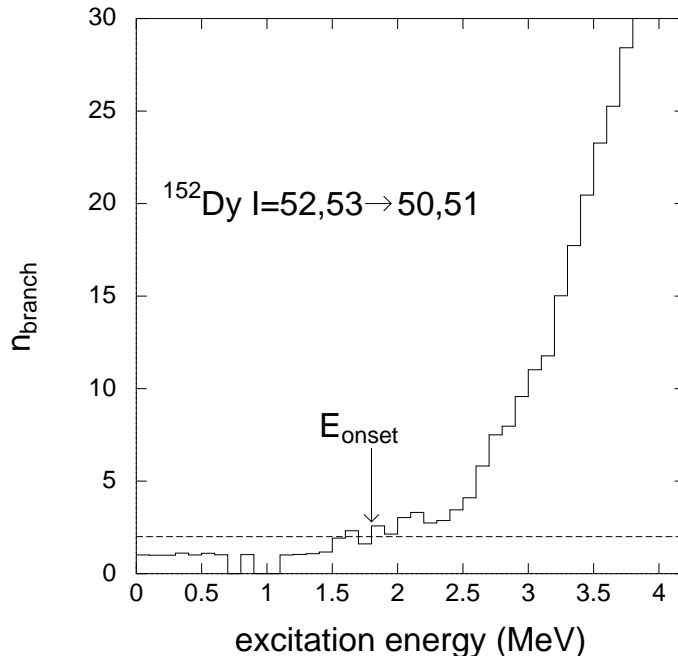


Figure 7: The branching number n_{branch} as a function of excitation energy above yrast line for ^{152}Dy , averaged over $I = 52^{\pm} \rightarrow 50^{\pm}$, $I = 53^{\pm} \rightarrow 51^{\pm}$. The horizontal lines shows $n_{\text{branch}} = 2$ used to define the onset of rotational damping.

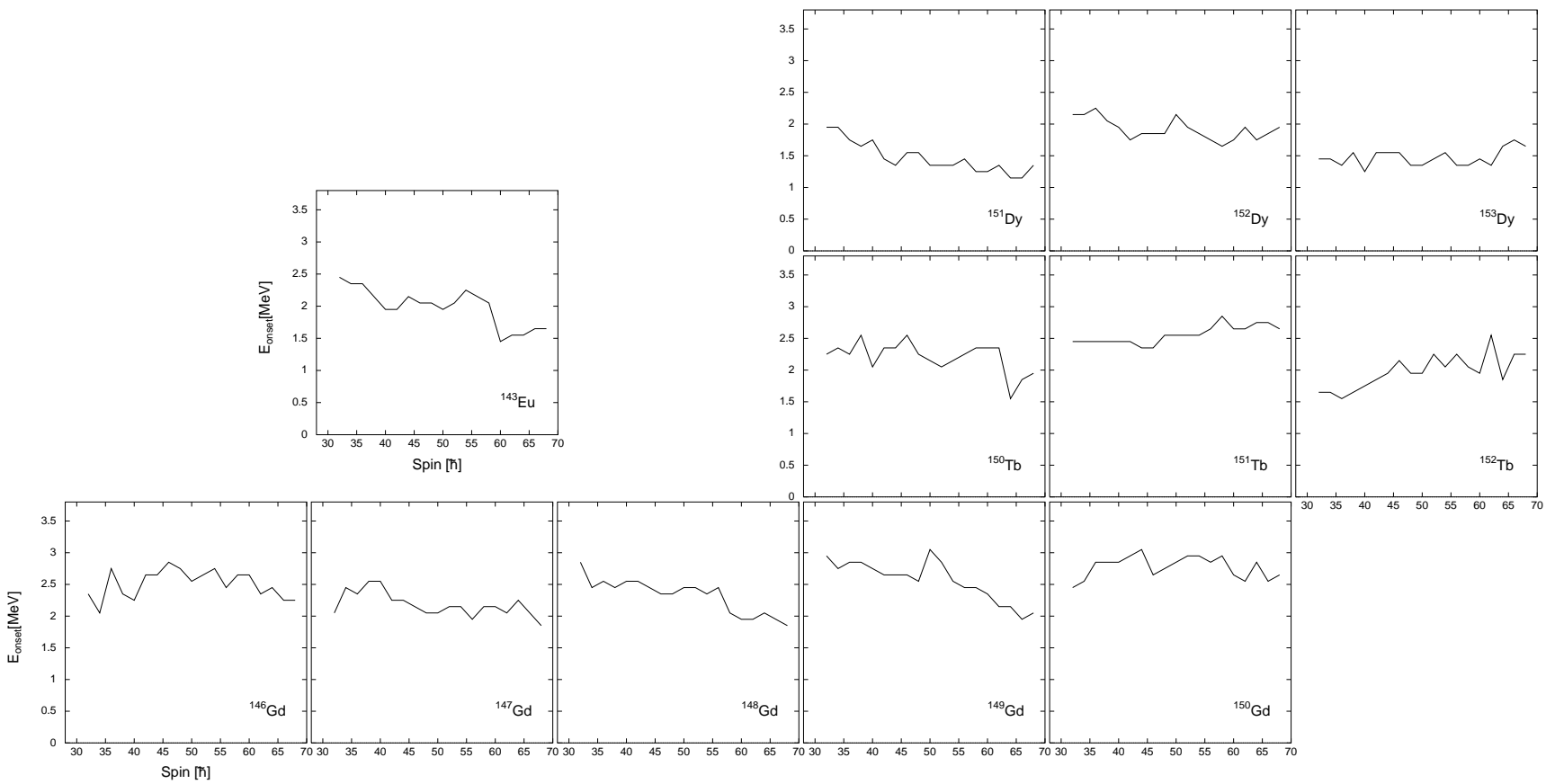
it may rather represent ambiguity of the definition of N_{band} . In order to see the dependence of the species, it is preferable to take averages of the onset energy E_{onset} and the number of bands N_{band} over different spins. Table. 3 summarizes the average E_{onset} and N_{band} where the averages are taken over spin range $I = 40 \sim 60\hbar$, which approximately correspond to spins where the superdeformed states are expected to dominate the yrast region.

It should be emphasized that, although the onset energy thus defined tells approximately where the rotational damping sets in, the transition from the rotational band structure to the rotational damping is not very sharp as function of excitation energy, but it develops rather gradually. As shown in Fig. 6, there are numerous "short bands" which are surrounded by the excited levels with damped rotational transitions. Because of the presence of such scars of rotational bands[22], the onset energy E_{onset} should be regarded as one of the measures defining the transition. In fact, the scars still exist at 1 MeV above the onset energy.

4.2 Discussion

The calculated onset energy E_{onset} for the superdeformed nuclei is about 1.5 ~ 3.0 MeV above yrast line, depending on species (Fig. 8 and Table. 3). It is significantly higher than the onset energy $E_{\text{onset}} \sim 0.8$ MeV in normal deformed rare-earth nuclei[6, 7]. The calculated number of bands $N_{\text{band}} \sim 40 - 70$, is also larger than the corresponding number $N_{\text{band}} \sim 30$ in normally deformed nucleus ^{168}Yb , while N_{band} in a few superdeformed nuclei such as ^{143}Eu and ^{151}Dy is comparable with that in normal deformed nuclei.

Figure 8: Onset excitation energy of rotational damping E_{onset} measured from the yrast line for each superdeformed nuclei, as a function of spin.



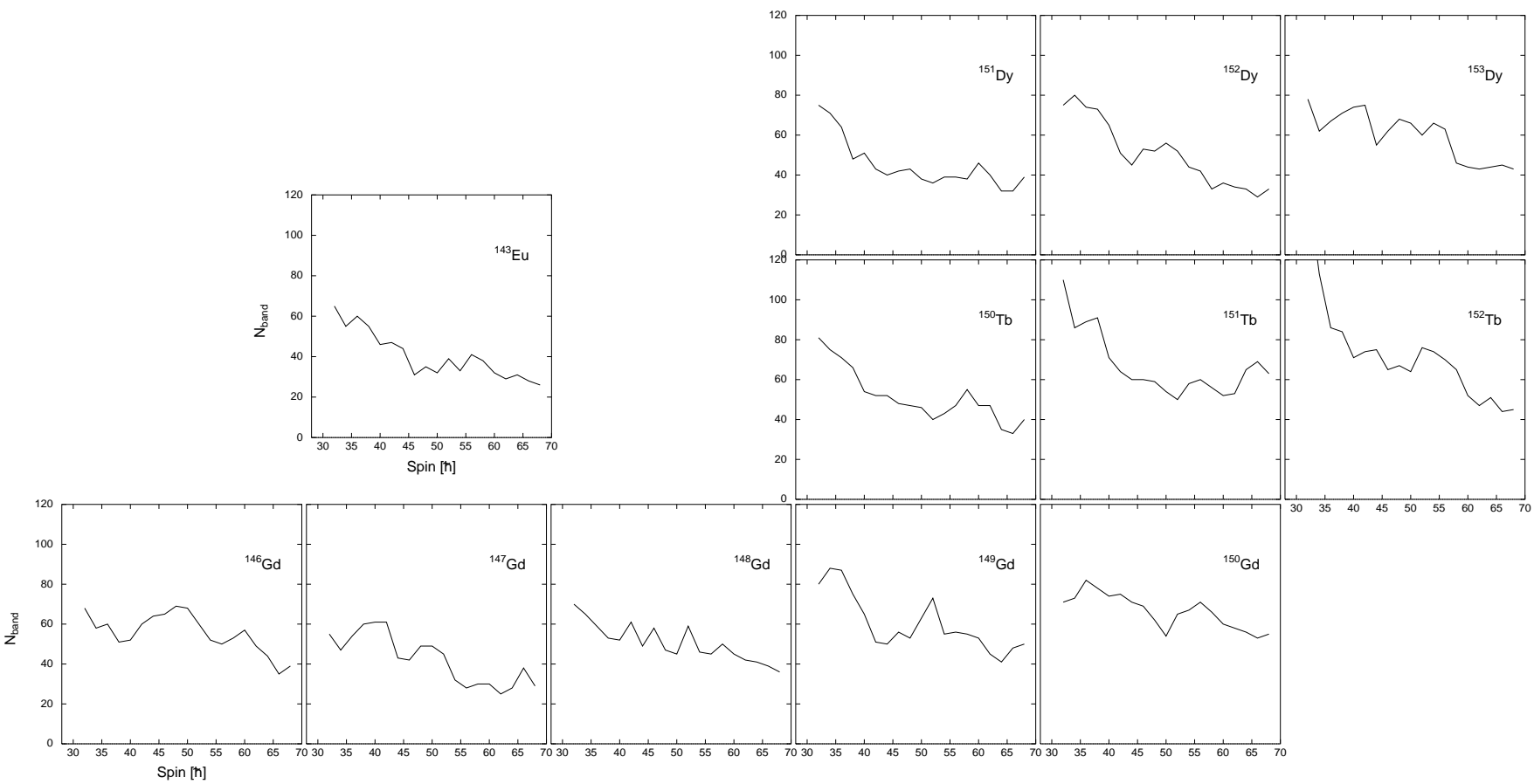


Figure 9: The calculated number of superdeformed bands N_{band} (see text for definition) as a function of spin for each superdeformed nucleus.

	E_{onset} [MeV]	N_{band}
^{143}Eu	2.0	38
^{146}Gd	2.7	60
^{147}Gd	2.1	41
^{148}Gd	2.3	51
^{149}Gd	2.6	57
^{150}Gd	2.9	66
^{150}Tb	2.3	48
^{151}Tb	2.6	57
^{152}Tb	1.7	67
^{151}Dy	1.4	40
^{152}Dy	1.8	46
^{153}Dy	1.5	60

Table 3: The calculated onset excitation energy E_{onset} of rotational damping measured from the yrast line, and the calculated number of superdeformed bands N_{band} , averaged over $I = 40\hbar \sim 60\hbar$.

Another characteristic feature seen from Fig. 8,9 and Table. 3 is variation of the onset energy and the number of bands in different superdeformed nuclei. For example, the onset energy becomes the highest (about 3.0 MeV) and the number of bands is also large (about 70) in ^{150}Gd , while the same quantities become a factor 1/2 small in ^{143}Eu (about 2.0 MeV and 40) and ^{151}Dy (about 1.4 MeV and 40). One can also trace that E_{onset} and N_{band} decrease as the neutron number decreases in Gd isotopes.

Both the difference from the normal deformed nuclei and the variation among the superdeformed nuclei are explained in terms of the characteristics of the level densities discussed in Sec. 3. In this connection, it is useful to recall the argument in Ref.[2] that the damping of rotational motion takes place if the spreading of unperturbed np - nh configurations is caused by the two-body residual interaction, which is represented by the condition $\Gamma_{\mu} > d_{2\text{body}}$. Here $\Gamma_{\mu} = 2\pi v^2 \rho_{2\text{body}}$ is the spreading width of np - nh configurations with v being the average size of matrix elements of the residual interaction, and $\rho_{2\text{body}}$ being the two-body level density. The spreading is meaningful only when it is larger than the spacing between interacting states $d_{2\text{body}} = \rho_{2\text{body}}^{-1}$. The above condition reads

$$\rho_{2\text{body}} > 1/\sqrt{2\pi}v \quad (19)$$

implying that the onset of the rotational damping is governed by the ratio between the two-body level spacing $d_{2\text{body}} = \rho_{2\text{body}}^{-1}$ and the two-body interaction strength. As $\rho_{2\text{body}}(E)$ increases with excitation energy, the rotational damping sets in at the excitation energy where the condition Eq. (19) is satisfied. It is now to be noticed that the two-body level density in superdeformed nuclei is much lower than in normally deformed nuclei as shown in Fig. 2. Assuming that the matrix elements of residual two-body interaction does not depend on deformation, the onset energy E_{onset} satisfying the condition Eq. (19) must be much larger in superdeformed nuclei than in normally deformed nuclei. The variation of E_{onset} among the superdeformed nuclei can be explained along the same argument. It is seen from combination of Table. 2 and Table. 3 that the variation of E_{onset} is correlated with that of the fitted level density parameters and the shell correction energy. For example, the onset energy E_{onset} , the fitted level density parameters and the shell correction energy become the largest in ^{150}Gd . In

this nucleus, the two-body level density becomes very small due to the shell gap at $N=86$ and $Z=64$ Fermi surfaces.

To be more quantitative, let us adopt the Fermi gas expression Eq. (16) for the two-body level density. Then the onset energy is estimated from Eq. (19) as

$$E_{\text{onset}} = 7.11\bar{v}^{-2/3}a^{-5/3}. \quad (20)$$

Choosing $v = 25$ keV and $a = A/10$ ($A = 170$), the onset energy in this estimate $E_{\text{onset}} = 0.74$ MeV agrees with the microscopic calculation for normally deformed nuclei[7]. With the same interaction strength, but with smaller level density parameter $a = A/15 \sim A/20$ ($A = 150$) corresponding to the superdeformed states, the estimate reads $E_{\text{onset}} = 1.8 \sim 2.9$ MeV, which roughly agrees with the microscopic results in Table. 3.

Let us now discuss the number of bands. The microscopic results are about $40 \sim 70$, which are about factor 1-2 larger than in normally deformed nuclei. The variation of N_{band} among the superdeformed nuclei is correlated to that of the level densities as seen from Table. 2 and Table. 3; the larger the number of bands is, the smaller are the level density parameters. For qualitative understanding of these features, let us utilize two schematic models. The first one is along the same line with the above discussion for E_{onset} . The number of bands in this model may be estimated by counting the levels up to the onset energy given by Eq. (20) provided that the boundary is sharp(while, in fact, this assumption is not necessarily correct as Fig. 6 indicates). Then the number of bands is given by

$$\begin{aligned} N_{\text{band}} &= 4 \int_0^{E_{\text{onset}}} \rho(E) dE \\ &= \frac{\sqrt{\pi}}{12} \int^{x_0} x^{-5/4} \exp 2\sqrt{x} dx, \\ x_0 &= 7.11(a\bar{v})^{-2/3}. \end{aligned} \quad (21)$$

Here the Fermi gas expression Eq. (15) for the total level density $\rho(E)$ is used. Multiplier 4 is needed to count different parity and signature states. The number of bands is an steeply increasing function of $(a\bar{v})^{-1}$;

$N_{\text{band}} = 26, 55, 100, 170, 270, 400$ for $(a\bar{v})^{-1} = 2, 3, 4, 5, 6, 7$. The choice of the interaction strength $v = 25$ keV gives $N_{\text{band}} = 34$ for a normally deformed nucleus with $A = 170$ in agreement with the microscopic calculation. With small level density parameters corresponding to the superdeformed nuclei, the estimate produces $N_{\text{band}} = 101 \sim 201$ for $a = A/15 \sim A/20$. This indicates the significant increase of the number of superdeformed bands and its sensitivity to the variation of level density. However this model apparently overestimates the microscopic results in Table. 3. The overestimate in N_{band} can be traced back to the fact already revealed that the density parameter a fitting the total level density $\rho(E)$ is significantly smaller than that for $\rho_{2\text{body}}(E)$. As is discussed in Sec. 3, the level densities affected by the presence of the shell gap in the single particle spectrum cannot be simulated simply by a single value of the the level density parameter. In order to treat the shell gap explicitly, let us next consider the other model, which simplifies the situation by assuming that the single-particle spectrum is uniform with density $\frac{1}{2}g_0$ (related to the level density parameter $a = \frac{\pi^2}{6}g_0$) except the presence of the gaps with interval Δ at the Fermi surface. Considering the limit of large Δ , the lowest excited levels are dominated only by 1p-1h excitations. In

this limit, the total level density $\rho(E)$ is significantly reduced, and is expressed as

$$\rho(E) = \rho_{2\text{body}}(E) = \frac{1}{2}g_0^2(E - \Delta) \quad (E > \Delta) \quad (22)$$

The two-body level density is the same as $\rho(E)$ since all the 1p-1h states can interact through the two-body force. With $v = 25$ keV and $a = A/10$ corresponding to the average single-particle density[20], the onset energy and the number of bands are estimated as

$$E_{\text{onset}} = \frac{4\sqrt{2}}{\sqrt{\pi}vg_0^2} + \Delta = 1.53\text{MeV} + \Delta, \quad (23)$$

$$N_{\text{band}} = \frac{8}{\pi v^2 g_0^2} = 49. \quad (24)$$

The onset energy E_{onset} increases with increase of the single-particle gap Δ while the estimated number of bands reaches to a constant independent of Δ , which is not very large comparing with an estimate $N_{\text{band}} = 44$ corresponding to $\Delta = 0$ ($a = A/10, A = 150$ in Eq. (21)). The two schematic models discussed above simplify the realistic features of the single-particle spectra for superdeformed potential. The calculated level densities presented in Sec. 3 seem to lie in-between the two models.

It should be reminded that the onset of rotational damping does not take place very sharply at the onset energy, but proceeds quite irregularly as function of the excitation energy, as is discussed in the preceding subsection and demonstrated in Fig. 6. This is because there are local fluctuation of the unperturbed levels and the matrix elements of the residual interactions depending on the configurations of the many-particle many-hole states. A little deviation of E_{onset} and N_{band} from the systematics expected from the N, Z -dependence of the shell structure effect in the single-particle levels may be due to such fluctuations.

We noticed, in Fig. 9, systematic spin dependence that the number of bands increases with decreasing spin below $40\hbar$. This spin dependence is not correlated with the level density since the calculated level densities in Fig. 4 and 5 have no systematic spin dependence which can explain the increase of N_{band} . This may indicate that the onset of rotational damping is not controlled by the configuration mixing alone. It is should be noticed in this connection that the alignment effect is also important to cause the rotational damping, while it is not very large for the low spin region in superdeformed nuclei. The dispersion of rotational frequency $2\Delta\omega$, which measures the alignment effect and represents how different rotational bands respond to the spin change of $\Delta I = 2$, is about 40 keV at $I = 30$ on the basis of the estimate of Ref. [2]. This is not sufficiently large than the scale of the residual interaction effects ~ 50 keV ($d_{2\text{body}} \sim \sqrt{2\pi}v$ at the onset energy), the rotational correlation persist more than expected from the argument based on the level densities. It is to be reminded that possible persistence of the rotational band structure in the region of strong configuration mixing is pointed out in Ref. [23].

4.3 Comparison with experiments

Recent experiments identify several superdeformed bands in a nucleus in $A \sim 150$ region[1]. Our microscopic calculation predicts at least more than ten superdeformed rotational bands even if "the short rotational bands" are excluded (there are three other figures in addition to the lower panel of Fig. 6 for ^{152}Dy). It implies that

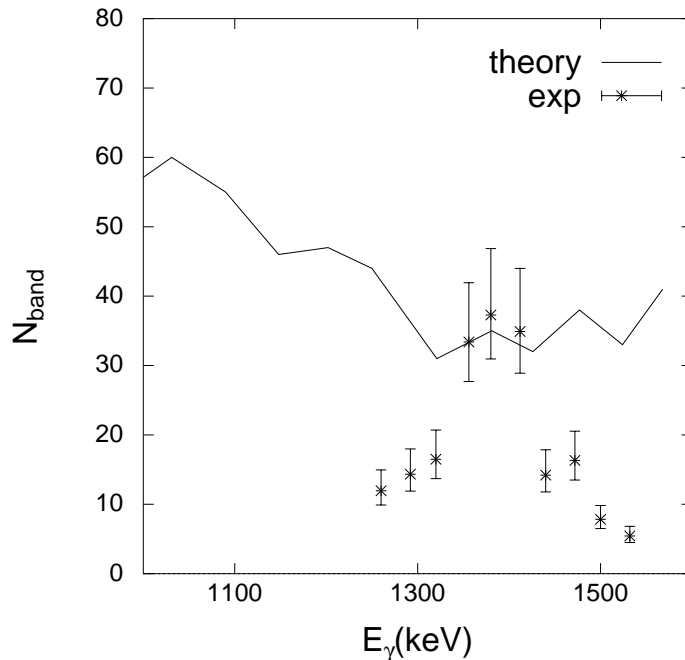


Figure 10: The experimental effective number of decay paths [10] and the calculated number of superdeformed bands N_{band} as a function of the transition gamma-ray energy.

the current spectroscopic studies of discrete gamma-ray peaks reaches far below the onset of rotational damping in superdeformed nuclei. In other words, the present calculation suggests possibility to find further number of superdeformed bands in a nucleus in future experiments.

Available experimental data concerning the the onset of rotational damping in superdeformed nuclei come from analysis of quasi-continuum part of double-coincident $E_{\gamma_1} \times E_{\gamma_2}$ spectra although the number of data is very limited so far. An indirect information comes from an simulation of the quasi-continuum gamma-rays in superdeformed ^{152}Dy [24], which points to an estimated value E_{onset} around $2.5 \sim 3.0$ MeV from the observed intensity of the ridge part of the $E_{\gamma_1} \times E_{\gamma_2}$ spectra [25]. This analysis agrees with the present microscopic calculation in the qualitative feature that the onset of damping takes place at much higher excitation energy than in normal deformed nuclei.

More direct information comes from the fluctuation analysis method which extracts the effective number of paths of decays from the quasi-continuum part of $E_{\gamma_1} \times E_{\gamma_2}$ spectra [3, 4]. When this method is applied to the first ridge of the spectra located at $E_{\gamma_1} - E_{\gamma_2} = \pm 4/\mathcal{I}$ lines with \mathcal{I} being the moment of inertia of superdeformed bands, the effective number of paths counts the number of two consecutive collective E2 transitions, $I+2 \rightarrow I \rightarrow I-2$. Thus the effective number of paths at the first ridge approximately corresponds to the number of bands which is defined in Sec. 2. The data for superdeformed nuclei is available only in ^{143}Eu [10]. Comparison between the theory and the experimental data is done in Fig. 10, in which our results is plotted as a function of the average gamma-ray energy. The data points are limited in the region $E_\gamma \sim 1250 - 1550$ keV where the quasi-continuum ridge is observed. The calculated

number of bands agrees with the experimental effective number of paths at around $E_\gamma \sim 1400\text{keV}$.

The effective number of paths becomes smaller around high and low ends of the measured E_γ range than the theoretical number of bands. This may suggest some other mechanisms that destroy rotational band structures in addition to the rotational damping. For example, for the region with $E_\gamma \gtrsim 1500$ keV corresponding to the very high spins $I \gtrsim 55\hbar$, the fission decay may compete with the collective E2 gamma decay and hinder the E2 decay branches[24]. Furthermore, feeding mechanism of the superdeformed states may affect the effective number of paths. The low gamma-ray energy $E_\gamma \lesssim 1300$ keV, on the other hand, corresponds to spins $I \lesssim 40\hbar$, at which the lowest superdeformed states lie higher in energy than the yrast line consisting of normally deformed states. Since the superdeformed states are surrounded by numerous normal deformed states in this situation, mixing between normal and superdeformed states may take place and cause breaking of rotational band structures of the superdeformed states. Inclusion of these effects has possibility to explain the data points, but it is beyond the scope of the present paper.

5 Conclusion

We analyzed the onset of the rotational damping in $A \sim 150$ superdeformed nuclei by means of the shell model diagonalization method comprised of the cranked Nilsson mean-field and the residual two-body interaction.

The rotational damping in superdeformed nuclei sets in at the excitation energy of about $2 \sim 3$ MeV above superdeformed yrast line. The onset energy is much higher than the theoretical prediction in normally deformed rare-earth nuclei. The effective number of rotational bands is calculated to be $40 \sim 70$, which is slightly larger than the corresponding number (about 30) in normally deformed nuclei. Both the onset energy and the number of bands show the variation depending on the superdeformed species even among $A \sim 150$ region.

All these features characteristic for the superdeformed nuclei are originated from the shell structure in the single-particle spectrum associated with the superdeformed shape of the mean-field potential. This was demonstrated explicitly by looking into the total level density as well as the two-body level density which is relevant to the configuration mixing via two-body forces. The shell gap in the single-particle spectrum causes significant decrease in the level densities in comparison with those in the normally deformed nuclei, and causes increase in the onset energy and the number of bands. Since the shell structure at the Fermi surface varies with neutron and proton numbers and associated changes in deformation, the level densities show significant dependence on superdeformed species even among $A \sim 150$ region. It causes the variation of the onset of rotational damping.

The calculated results are consistent with existing data. More systematic comparison with data is required, however, in order to check the predictions such as the mass-number dependence, and also to clarify other mechanisms which are not included in the present theory.

Acknowledgment

Discussions with S. Leoni, B. Herskind, T. Døssing, E. Vigezzi, R.A. Broglia and K. Matsuyanagi are greatly acknowledged. We also thank Y.R. Shimizu for discussion and for providing us the liquid-drop code. Numerical computation in this research was supported in part by Research Center for Nuclear Physics(RCNP), Osaka University, and the Institute for Chemical and Physical Research (RIKEN). A part of the numerical computations was carried out at RIKEN.

Appendix

In order to calculate the two-body level density $\rho_{2\text{body}}(E)$, it is useful to define a related quantity

$$\rho^{(2)}(E_1, E_2) = \sum_{\mu\mu'}' \delta(E_1 - E_\mu)\delta(E_2 - E_{\mu'}) \quad (25)$$

where $\sum_{\mu\mu'}'$ denotes the summation over pairs of np - nh states which interact via two-body residual interaction. Eq. (25) can be rewritten as

$$\rho^{(2)}(E_1, E_2) = \sum_{\mu} \delta(E_1 - E_\mu) \sum_{\mu'(\mu)}' \delta(E_2 - E_{\mu'}) \quad (26)$$

$$= \sum_{\mu} \delta(E_1 - E_\mu) \rho_{2\text{body}}(\mu, E_2) \quad (27)$$

$$= \rho(E_1) \rho_{2\text{body}}(E_1, E_2) \quad (28)$$

Here the quantity $\rho_{2\text{body}}(\mu, E_2)$ representing density of states coupled with the state μ via the two-body interaction is assumed to depend only on the energy E_μ of the state. Then the two-body level density is given by

$$\begin{aligned} \rho_{2\text{body}}(E) &= \rho_{2\text{body}}(E, E) \\ &= \rho^{(2)}(E, E) / \rho(E) . \end{aligned} \quad (29)$$

In numerical calculation, the delta functions in Eq. (25) is replaced by an Gaussian function used in the Strutinsky averaging. The level density $\rho(E) = \sum_{\mu} \delta(E - E_\mu)$ is also calculated with the same Gaussian function. The width of the Gaussian function used in the numerical calculation is 200 keV.

References

- [1] P.J. Dagnall, C.W. Beausang, P.J. Twin, M.A. Bentley, F.A. Beck, Th. Byrski, S. Clarke, D. Curien, G. Duchene, G. de France, P.D. Forsyth, B. Haas, J.C. Lisle, E.S. Paul, J. Simpson, J. Styczen, J.P. Vivien, J.N. Wilson, and K. Zuber, Phys. Lett. **B335**(1994)313.
As a compilation of observed excited superdeformed bands, see *Table of Superdeformed Nuclear Bands and Fission Isomers* edited by B. Singh, R.B. Firestone, and S.Y.F. Chu ,LBL-38004(Lawrence Berkeley National Laboratory,1995).
- [2] B. Lauritzen, T. Døssing, and R.A. Broglia, Nucl. Phys. **A457**(1986)61.

- [3] B. Herskind, A. Bracco, R.A. Broglia, T. Døssing, A. Ikeda, S. Leoni, J. Lisle, M. Matsuo, and E. Vigezzi, Phys. Rev. Lett. **68**(1992)3008;
T. Døssing, B. Herskind, S. Leoni, M. Matsuo, A. Bracco, R.A. Broglia, and E. Vigezzi, Physics Reports (1996) to be published.
- [4] B. Herskind, T. Døssing, S. Leoni, M. Matsuo, and E. Vigezzi, Prog. Part. Nucl. Phys. Vol.28 (Pergamon, 1992)p.235;
B. Herskind, T. Døssing, S. Leoni, M. Matsuo, N. Nica, D.C. Radford, and P.Rasmussen, Nucl. Phys. **A557**(1993)191c;
H. Herskind, S. Leoni, T. Døssing, G.B. Hagemann, P. Bosetti, A. Bracco, S. Frattini, E. Vigezzi, and M. Matsuo, Acta Physica Polonica **B26**(1995)153.
- [5] S.Åberg, Phys. Rev. Lett. **64**(1990)3119;
S.Åberg, Prog. Part. Nucl. Phys. vol.28 (Pergamon,1992)p11.
- [6] M. Matsuo, T. Døssing, E. Vigezzi and R.A. Broglia, Phys. Rev. Lett. **70** (1993)2694.
- [7] M. Matsuo, T. Døssing, E. Vigezzi, R.A. Broglia, and K. Yoshida, in preparation.
- [8] S. Åberg, Nucl. Phys. **A477**(1988)18.
- [9] T.R. Werner and J. Dudek, Phys. Rev. **C44**(1991)R948.
- [10] S. Leoni, B. Herskind, T. Døssing, K. Yoshida, M. Matsuo, A. Ataç, G.B. Hagemann, F. Ingebresten, H.J. Jensen, R.M. Lieder, G.V. Marti, N. Nica, J. Nyberg, M. Piparinen, H. Schnare, G. Sletten, K. Stähle, M. Sugawara, P.O. Tjøm, and A. Virtanen, Phys. Lett. **B353**(1995)179.
- [11] S. Nilsson, C.F. Tsang, A. Sobiczewski, Z. Szymanski, S. Wycech, C. Gustafson, I. Lena, P. Møller, and B. Nilsson, Nucl. Phys. **A131**(1969)1.
- [12] T. Bengtsson and I. Ragnarsson, Nucl. Phys. **A436**(1985)14.
- [13] T.Bengtsson, Nucl. Phys. **A496**(1989)56.
- [14] T. Bengtsson, I. Ragnarsson and S. Åberg, Phys. Lett. **B208**(1988)39;
P. Fallon, P. Alderson, M.A. Bentley, A.M. Bruce, P.D. Forsyth, D. Howe, J.W. Roberts, J.F. Sharpey-Schafer, P.J. Twin, F.A. Beck, T. Byrski, D. Curien and C. Schuck, Phys. Lett. **B218**(1989)137.
- [15] G. Anderson, S.E. Larsson, G. Leander, P. Møller, S.G. Nilsson, I. Ragnarsson, S. Åberg, R. Bengtsson, J.Dudek, B. Nerlo-Pomorska, K. Pomorski, and Z. Szymanski, Nucl. Phys. **A268**(1976)205.
- [16] P. Ring and P. Shuck, *The Nuclear Many Body Problem* (Springer-Verlag, 1980).
- [17] W.D. Myers and W.J. Swiatecki, Arkiv Fysik **36**(1967)343 ;
S. Cohen, F. Plasil and W.J. Swiatecki, Ann. Phys. **82**(1974)557.
- [18] I.M. Green and S. A. Mozkowski, Phys. Rev. **139**(1965)B790;
R. Arvieu and S.A. Mozkowski, Phys. Rev. **145**(1966)830.
- [19] A. Faessler, Fortschr. Phys. **16**(1968)309 .
- [20] A. Bohr and B.R. Mottelson, *Nuclear Structure*. vol. I (Benjamin, 1969).
- [21] T. Ericson, Advances in Physics **9**(1960)425.
- [22] R.A. Broglia, T. Døssing, M. Matsuo, E. Vigezzi, P. Bosetti, A. Bracco, S. Frattini, B. Herskind, S. Leoni, and P. Rasmussen, submitted to Phys. Rev. Lett.

- [23] B.R. Mottelson, Proc. Intern. Seminar on The Frontier of Nuclear Spectroscopy(Kyoto) (World Scientific, 1992)p7;
B.R. Mottelson, Nucl. Phys. **A557**(1992)717c.
- [24] K. Schiffer and B. Herskind, Phys. Lett. **B255** (1991)508;
K. Schiffer and B. Herskind, Nucl. Phys. **A520**(1990)521c.
- [25] P.J. Twin, Proc. Intern. Conf. on Nuclear shapes(Creta) (World Scientific, 1988)p152;
P.J. Twin, Nucl. Phys. **A520**(1990)17c.